



Towards chip prototyping: a model for droplet formation at both T and X-junctions in dripping regime

Axel Vansteene¹ · Jean-Philippe Jasmin¹ · Siméon Cavadias^{2,3} · Clarisse Mariet¹ · Gérard Cote²

Received: 4 December 2017 / Accepted: 18 May 2018 / Published online: 31 May 2018
© Springer-Verlag GmbH Germany, part of Springer Nature 2018

Abstract

Segmented flows in both T and X-junction glass microchannels are investigated. The effective pressure domain of use of the microchips are compared for two chemical systems. After studying the flow patterns and current empirical equations proposed in the literature, a new empirical equation is validated for both T and X-junctions allowing the prediction of not only the domain of use of the microchip in terms of flow rates knowing the viscosities of the two phases but also the droplets diameter, volume, spacing, and specific interfacial area. Specific interfacial area could be optimized using the model within our specific microsystems, and a maximum of $10,000 \text{ m}^{-1}$ is determined. Ensuing the definition of the model, several insights in the way to optimize segmented flows for different purposes are discussed, i.e., for the production of monodisperse populations of droplets and mass transfer optimization.

Keywords Solvent extraction · Microfluidics · Lab-on-chip · Hydrodynamics · Modelling · Uranium · Europium

List of symbols

$(\alpha_{\text{lag}}, \alpha_{\text{fill}}, \beta)$	Parameters defined in Glawdel et al. (Eq. 11) and Chen et al. (Eq. 12) comprehensive models	FF	Focalized flux-junction
$\bar{\beta}$	Parameter defined in Sessoms et al. (Eq. 14) for the velocity of the unconfined droplets	fps	Frame per second (s^{-1})
(χ_1, χ_2, χ_3)	Fitting parameters of our empirical equation	h	Channel height (m)
Ca	Capillary number	H	Distance between the inlet of the dispersed phase and the orifice in FF-junctions
Ca'	Modified capillary number	ID	Internal diameter (m)
DMDBDTMA	<i>N,N'</i> -Dimethyl <i>N,N'</i> -dibutyl tetradecylmalonamide	L	Length of a microchannel (m)
f	Droplet generation frequency (Hz)	l	Diameter/Length of the droplet/plug (m)
		O	Oil
		P	Pressure (Pa)
		PEEK	Polyether ether ketone
		Q	Flow-rate ($\text{m}^3 \text{ s}^{-1}$)
		S	Surface (m^2)
		s	Spacing between consecutive droplets (m)
		$S_{\text{int,spec}}$	Specific interfacial area (m^{-1})
		T	T-junction
		U	Average superficial velocity (m s^{-1})
		v	Velocity (m s^{-1})
		W	Water
		w	Channel width (m)
		X	Cross junction
		Γ	Height-to-width ratio of the junction/aspect ratio h/w
		δP	Variation of inlet pressure (Pa)
		$\Delta r/r$	Relative error (%)
		η	Dynamic viscosity (Pa s)

Electronic supplementary material The online version of this article (<https://doi.org/10.1007/s10404-018-2080-2>) contains supplementary material, which is available to authorized users.

✉ Clarisse Mariet
clarisse.mariet@cea.fr

¹ Den-Service d'Etudes Analytiques et de Réactivité des Surfaces (SEARS), CEA, Université Paris-Saclay, 91191 Gif-sur-Yvette, France

² Institut de Recherche de Chimie Paris, Chimie ParisTech-CNRS, PSL Research University, 75005 Paris, France

³ UPMC-Univ Paris 06, 4 Place Jussieu, 75005 Paris, France

λ	Viscosity ratio η_d/η_c
Λ	Dispersed-to-continuous channel width ratio w_d/w_c
σ	Interfacial tension (N m^{-1})
Φ	Flow-rate ratio Q_d/Q_c

Subscripts

c	Continuous phase
channel	Outlet microchannel
d	Dispersed phase
exp	Experimental
max	Maximum value
mean	Average value
min	Minimum value
or	Orifice in FF-junctions
plot	Related to the droplet or plug
targeted	Targeted value
th	Theoretical
tot	Total

1 Introduction

Droplet-based microsystems have found numerous applications in DNA analysis, encapsulation of macromolecules and cells, protein crystallization, synthesis of nanoparticles, microparticles, and colloidal assemblies, chemical reaction networks, formulation (Song et al. 2006). Compared to conventional techniques that use reaction vessels, test tubes or microliter plates, microfluidic technology offers several unique advantages: (1) minimized volumes of sample or reagents and reduced costs; (2) increased volumetric mass transfer coefficient thanks to high surface-to-volume ratios and inner slug recirculations; (3) possible mass parallelization and automation. Moreover, segmented flows enhance mixing, increase mass transfer and reduce dispersion (Hessel et al. 2005) and allow to achieve increased performance relative to conventional bench scale systems (Song et al. 2003; Zheng and Ismagilov 2005; Hatakeyama et al. 2006). The mass transfer is improved both by the increase of the specific interfacial area (Ahmed et al. 2006; Fries et al. 2008; Assmann et al. 2013) and by the recirculation of the compounds (Burns and Ramshaw 2001) through the generation of segmented flows.

Two-phase flows are encountered on an industrial scale, in areas as varied as the classical hydrometallurgy, the nuclear industry, the petrochemical industry, the pharmaceutical industry or the agri-food industry. To improve mass transfer during the liquid–liquid extraction, a solution consists in the optimization of the specific interfacial area with the formation of segmented flows. Discrete droplets can be produced in a continuously flowing immiscible liquid, and manipulated

by downstream changes in the flow, either passively via bifurcations or constrictions (Boyd-Moss et al. 2016). The active methods (Chong et al. 2015; Zhu and Wang 2016) are excluded from the scope of this article. (Dreyfus et al. 2003). When immiscible fluid streams are contacted at the inlet section of a microchannel, the ultimate flow regime depends on geometry, surface properties (Aota et al. 2007; Kralj et al. 2007; Shui et al. 2007; Anna 2016), flow rates (Kashid et al. 2011; Sen et al. 2014), and both phases physico-chemical properties (mostly viscosity and surface tension between the two phases). This multitude of influential parameters offers a lot of control over droplet formation but, due to the absence of adequate (i.e., quantitatively predicting) theoretical models, each new combination of geometry, speeds and viscosities may need to be explored and tuned, to adjust droplet size and formation rate. Therefore, many studies (Christopher and Anna 2007) examine the mechanisms for droplet breakup in co-flow (Umbanhowar et al. 2000; Utada et al. 2007), T (Tice et al. 2004; Garstecki et al. 2006; Xu et al. 2006a, b, c; Liu and Zhang 2009; Glawdel et al. 2012a, b), flow focusing (Garstecki et al. 2005), and cross-flow (Cubaud and Mason 2008; Liu and Zhang 2011; Fu et al. 2012) junctions to establish comprehensive models (Glawdel et al. 2012a, b; Chen et al. 2014) which can be generalized for different physico-chemical properties of the phases or junction geometry. Notably, simple models for the droplet size have been presented in the last decade for various T (Garstecki et al. 2006; Xu et al. 2006a, b, c, 2008; Gupta and Kumar 2009, 2010; van Steijn et al. 2010; Glawdel et al. 2012a, b) flow-focusing (Fu et al. 2012; Romero and Abate 2012; Gupta et al. 2014) and cross junctions (denoted hereafter X) (Cubaud and Mason 2008; Liu and Zhang 2011; Chen et al. 2014; van Loo et al. 2016), highlighting different droplet creation regimes, mainly squeezing, transition, dripping and jetting. However, these models were found to be very specific regarding their own datasets, and, to our knowledge, no thorough comparison between various types of junctions was yet carried out in a given flow regime.

In this article, droplet generation was compared for two chemical systems, two types of junction, and different wettability of the microchannels. A simple predictive model, depending on the capillary number of the continuous phase and the flow-rate ratio and allowing the optimization of the specific interfacial area, was established for both junction types (T, X). Once validated in the dripping regime, this model gave us insights in the control of flow parameters as a mean for the optimization of both droplet production frequency and value of the specific interfacial area that will be used to optimize mass transfer in liquid–liquid extraction.

2 Experiments

In this section, we present the microsystems used for the study of the hydrodynamics of segmented flows, as well as the two studied chemical systems.

2.1 Experimental setup

A schematized experimental setup is presented (Fig. 1). Two Mitos P-Pumps (Dolomite, UK) were used to feed the aqueous and organic phases into two types of commercial glass chips (Dolomite, UK): a T-junction and a X-junction with rectangular microchannels (Table 1). Hydrophilic and hydrophobic microfluidic chips were used in this study to produce O/W and W/O emulsions, respectively. Flow channels of the hydrophilic chip were made of ultra-smooth glass surface which is naturally hydrophilic. Whereas in the case of hydrophobic chip, the ultra-smooth glass channels were hydrophobized using silanization (Kole and Bikkina 2017) (contact angles measurements are presented in supplementary material). Pressure-driven flow is accomplished using gas pressure cylinders, in which a regulator controls the imposed pressures of the to-be-dispersed phase and the continuous one, P_d and P_c , respectively. In the following the height-to-width ratio will be stated as Γ ($h_{channel}/w_{channel}$, commonly denoted as aspect ratio) and the dispersed-to-continuous channel width ratio will be stated as Λ (w_d/w_c) (Fig. 2). The chips microchannels exhibited different hydrophilicities allowing to create both oil in water (O/W) and water in oil (W/O) dispersions.

The outlet channel length (in which segmented flows occurred) comprised two sections, one of which being the

Table 1 Used droplet junction chips, $\Gamma = \Lambda = 1$

Chip	Chip name	Wettability
A	Droplet junction chip—T-junction	Hydrophobic
B	Droplet junction chip—X-junction	Hydrophobic
C	Droplet junction chip—T-junction	Hydrophilic
D	Droplet junction chip—X-junction	Hydrophilic

$w_d=100 \mu\text{m}$ and $w_c=100 \mu\text{m}$ are the widths of the microchannel for the inlet of the dispersed or the continuous phases, respectively. $w_{channel}=300 \mu\text{m}$, $h_{channel}=100 \mu\text{m}$, $L_{channel}=1.125 \text{ cm}$ are the width, the height and the length of the outlet microchannel, respectively

microchannel itself with a length $L_{channel}$ (Fig. 1), and the other being a PEEK (for hydrophobic microchips) or PEEK-SIL (for hydrophilic microchips) tubing from the chip to the phase separator, which length also varied in our experiments (10, 20, 50 cm). This tubing, purchased from IDEX Health & Science (GMBH, Germany) was chosen to match the section (0.2 mm ID for droplet junction chips) and surface properties (hydrophilicity) of the microchannel, to prevent any disruption in the segmented flow. After the outlet tubing, an Asia FLLEX module (Syrris Ltd., UK) was used as a continuous phase separator, operated via the application of a cross-membrane pressure. The organic segmented flow was therefore forced to cross the membrane, and, depending on the volume ratio of the two phases, pure phases could be collected at the outlet of the module.

A high-speed camera Mini AX-100, (Photron, England) was mounted on a digital inverted microscope DEMIL LED (Leica, France) equipped with an objective lens with a 40 times magnification to image directly the segmented flow in the microchannel with adjustable frame rate, from

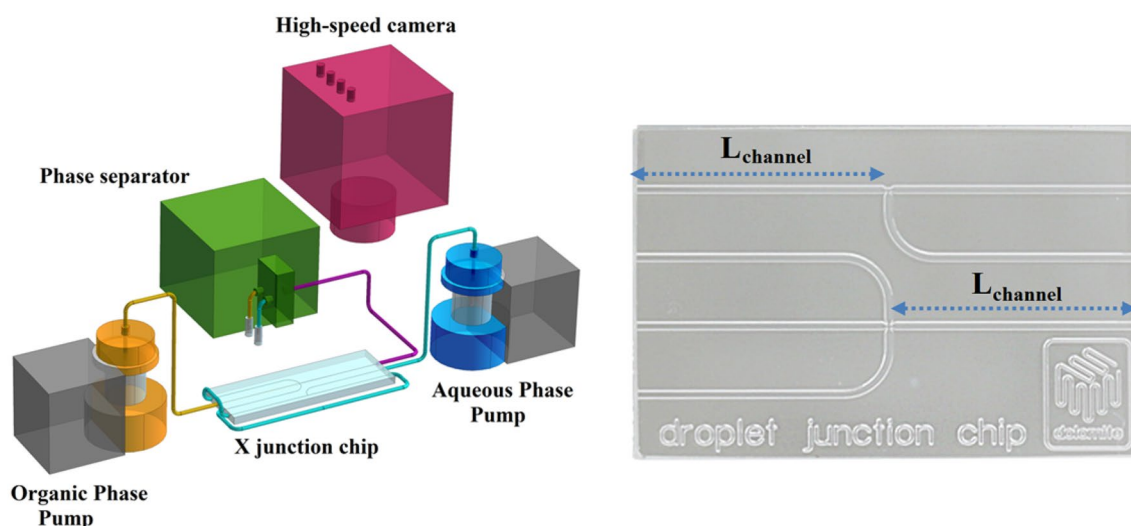
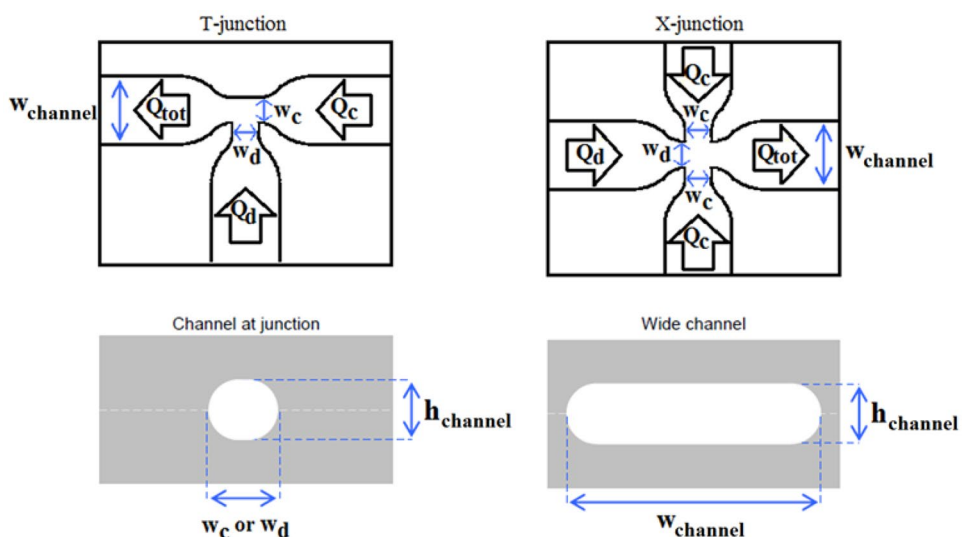


Fig. 1 Sketch of the experimental set-up. The outlet capillary (pink) was chosen to match the section of the outlet microchannel, and various lengths (10, 20, 50 cm) were tested. The various parameters characterizing the junctions are given on Fig. 2. (Color figure online)

Fig. 2 Geometric parameters characterizing the T and X-junctions



2,000 to 10,000 fps depending on droplet velocities. The recorded videos were analyzed using a Droplet Morphometry and Velocity software (Basu 2013), which provided droplets diameter, spacing and velocities. The ADM software (Chong et al. 2016) was also tested. Despite its speed and accuracy, it was found less user-friendly and lacked some post-processing tools, compared to the DMV software.

After each set of experiments, the microchannel was cleaned with isopropanol to remove any residual organic liquid and then flushed with compressed air.

2.2 Preparation and characterization of the solutions

N,N'-Dimethyl *N,N'*-dibutyl tetradecylmalonamide (DMD-BTDMA) (98.8%) was synthesized by Pharmasynthese SAS. The commercial extractant Aliquat[®] 336 (98%) was purchased from Alfa Aesar. HDEHP (99%), 1-decanol (99%) and *n*-dodecane were supplied by Sigma Aldrich. The extractants were all used as received. All aqueous solutions were prepared with 18-M Ω deionized water produced by a

Milli-Q water purification system (Millipore, Bedford, MA). Eu(NO₃)₃(H₂O)_{*n*}, HNO₃ 68% and HCl Ultrex 37% were purchased from Sigma Aldrich.

The determination, in batch at the equilibrium, of the optimal chemical conditions for the extraction were performed in a previous study (Hellé et al. 2014) for two chemical systems: Eu(III)/HNO₃/DMD-BTDMA and U(VI)/HCl/Aliquat[®] 336. The optimal compositions are [Eu(III)] = 10⁻² mol L⁻¹, [HNO₃] = 4 mol L⁻¹, [DMD-BTDMA] = 1 mol L⁻¹ in *n*-dodecane and [U(VI)] = 10⁻⁵ mol L⁻¹, [HCl] = 5 mol L⁻¹, [Aliquat[®] 336] = 10⁻² mol L⁻¹, in *n*-dodecane.

The hydrodynamic properties of these chemical systems were investigated without the analytes, nor surfactants. The solution densities and dynamic viscosities were measured using a DMA 4500 density-meter (Anton Paar, Austria) and a rotational automated viscosimeter Lovis 2000 M/ME (Anton Paar, Austria), respectively (Table 2). Interfacial tensions were measured using a tensiometer K100C (KRÜSS GmbH, France) by Du Noüy ring method.

For each junction chip, the chemical systems allowing for a continuous phase wetting of the microchannels were used and global systems mentioned as A₁, A₂, A₃, B₁, B₂, B₃, C₄,

Table 2 Physico-chemical properties of the fluids

Chemical system	Dispersed phase	Continuous phase	η_d (mPa s)	η_c (mPa s)	σ (mN m ⁻¹)	λ
1	[HNO ₃] = 4M	[DMD-BTDMA] = 1 M/dodecane	1.131 ± 0.001	20.27 ± 0.01	6.1 ± 0.1	0.056 ± 0.001
2	H ₂ O	Dodecane	0.998 ± 0.005	1.402 ± 0.001	18.5 ± 0.1	0.712 ± 0.004
3	[HCl] = 5 M	[Aliquat [®] 336] = 10 ⁻² M/dodecane	1.258 ± 0.001	1.382 ± 0.001	3.2 ± 0.1	0.910 ± 0.001
4	[Aliquat [®] 336] = 10 ⁻² M/dodecane	[HCl] = 5 M	1.382 ± 0.001	1.258 ± 0.001	3.2 ± 0.1	1.099 ± 0.002
5	[DMD-BTDMA] = 1 M/dodecane	[HNO ₃] = 4 M	20.27 ± 0.01	1.131 ± 0.001	6.1 ± 0.1	17.92 ± 0.03

η_d and η_c are the dynamic viscosities of the dispersed and continuous phases, respectively. σ is the interfacial tension between of the dispersed and continuous phases. λ denotes the viscosity ratio η_d/η_c for a given chemical system

C₅, D₄, D₅ are referring to both a junction type (Table 1) and a chemical system (Table 2).

2.3 Determination of the effective domain of use of the microchips

For each global system, droplet generation could be achieved. However, the quality of the dispersion strongly depended on the privileged wetting of the microchannel walls by the continuous phase. Then, the behavior of chemical system *i* was investigated only for the global systems A_{*i*} and B_{*i*} with *i* ≤ 3 or C_{*i*} and D_{*i*} with *i* > 3 (the identification of systems (i.e., A₁, A₂) refers to a specific chip from Table 1 and chemical system from Table 2).

Prior to the study of the flow regimes in the different junctions, the fields of use of the biphasic systems Eu(III)/HNO₃/DMDBTDMA and U(VI)/HCl/Aliquat® 336 have been characterized to determine the limits of applicable pressure to form segmented flow with the experimental setup described in Fig. 1.

Regardless of the junction (T or X), for a given pressure imposed on the continuous phase *P_c*, a minimum value of the pressure has to be imposed on the to-be-dispersed phase *P_{d,min}* to trigger droplet generation (Cubaud and Mason 2008; van Steijn et al. 2010; Glawdel et al. 2012a, b; Chen et al. 2014). Flows were observed for different pairs of pressures imposed on the two phases *P_c* and *P_d*. Figure 3, associated to an outlet capillary length of 50 cm, shows a linear dependence between *P_c* and *P_{d,min}* for the D₄ and D₅ global systems. It was found that for a given *P_c*, there also exist a maximum value, *P_{d,max}*, to impose on the to-be-dispersed phase, to prevent coalescence or jetting (at high flow rates) to happen. Similar results were obtained for the other global systems (Table 3). Every flow map, associated to a particular global system, was determined, and characterized by the mean difference of pressures δP_d , between the two straight lines defining the droplet generation region. For a given global system, only small variations of δP_d were found while changing the outlet capillary length (10, 20, 50 cm). Therefore, a mean value of δP_d for the different global systems was defined (Table 3).

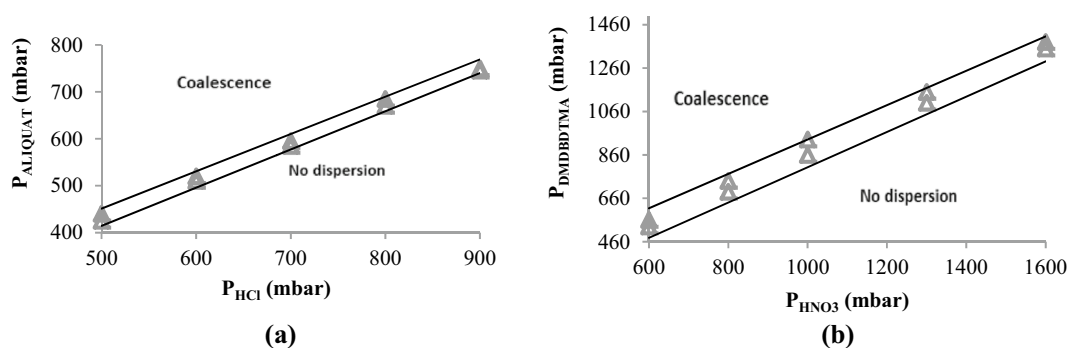


Fig. 3 Droplet generation field of use for **a** the D₄ and **b** the D₅ global systems, with the droplet generation region (between the two lines) and recorded experiments (Δ), for an outlet capillary length of 50 cm.

In the field “no dispersion”, no droplet was formed and back flow was observed in the to-be-dispersed phase. In the “coalescence zone” droplets are formed but eventually coalesce

Table 3 Difference of pressures, flow rates and capillary numbers characterizing droplet generation region, depending on specific global systems

Global system	A ₁	A ₂	A ₃	B ₁	B ₂	B ₃	C ₄	C ₅	D ₄	D ₅
δp (mbar)	35	10	30	20	45	35	10	55	35	115
$Q_{d,min}$ (mL h ⁻¹)	5.8.10 ⁻³	9.4.10 ⁻²	2.8.10 ⁻²	2.1.10 ⁻²	0.17	5.3.10 ⁻²	3.9.10 ⁻²	2.4.10 ⁻²	7.9.10 ⁻²	3.3.10 ⁻²
$Q_{d,max}$ (mL h ⁻¹)	0.17	1.1	0.51	0.43	1.1	0.54	0.18	0.12	0.58	0.24
Ca _{d,min}	3.8.10 ⁻⁵	1.8.10 ⁻⁴	3.8.10 ⁻⁴	1.4.10 ⁻⁴	3.2.10 ⁻⁴	7.4.10 ⁻⁴	6.0.10 ⁻⁴	2.8.10 ⁻³	1.2.10 ⁻³	3.9.10 ⁻³
Ca _{d,max}	1.1.10 ⁻³	2.1.10 ⁻³	7.1.10 ⁻³	2.8.10 ⁻³	2.1.10 ⁻³	7.5.10 ⁻³	2.8.10 ⁻³	1.5.10 ⁻²	8.9.10 ⁻³	2.8.10 ⁻²
$Q_{c,min}$ (mL h ⁻¹)	7.0.10 ⁻²	3.6	0.24	0.15	2.7	0.42	1.5	1.8	1.6	1.3
$Q_{c,max}$ (mL h ⁻¹)	1.9	7.6	7.9	2.1	8.3	4.1	8.7	6.6	6.1	11
Ca _{c,min}	8.2.10 ⁻³	9.5.10 ⁻³	3.7.10 ⁻³	1.8.10 ⁻²	7.2.10 ⁻³	6.4.10 ⁻³	2.1.10 ⁻²	1.2.10 ⁻²	2.2.10 ⁻²	8.4.10 ⁻³
Ca _{c,max}	0.23	2.0.10 ⁻²	0.12	0.24	2.2.10 ⁻²	6.3.10 ⁻²	0.12	4.3.10 ⁻²	8.4.10 ⁻²	7.3.10 ⁻²

The identification of systems (i.e., A₁, A₂) uses one device from Table 1 and one chemical system from Table 2

Experimentally, keeping a dispersion steady with $\delta P_d \leq 15$ mbar is extremely challenging (for example for A₂ and C₄ global systems). The hydrophilic T-junctions were investigated nevertheless, but are not ideal conditions for making stable organic droplets, due to partial wetting of the dispersed phase on the microchannel walls. O/W dispersions should rather be created in the X-junction chip.

2.4 Characterisation of the segmented flows

For the given limitations on the flow-rates (Table 3), droplet populations were created within each junction, and flow patterns were identified. Regime identification was carried out using generated sequences of droplet generation and derived flow rates of the continuous and dispersed phases. These flow-rates were acquired using the following methodology.

While using a pressure control on the fluids, the collection of the phases was completed, to deduce the total flow rate Q_{tot} :

$$Q_{tot} = Q_c + Q_d, \tag{1}$$

where Q_c and Q_d are the flow rates of the continuous and dispersed phases, respectively. The dispersed and continuous phases were collected in pre-weighted aliquots for a given duration Δt . Hence the total flow-rate was acquired by measuring the mass of the aliquots after the experiments.

The flow rate of the dispersed phase was deduced from the morphometry and velocity analysis of our experiments:

$$Q_d = V_{plot} \times f, \tag{2}$$

where f is the droplet generation frequency, obtained via the analysis of droplet generation sequences acquired through the use of the high-speed camera, and V_{plot} refers to droplets volume.

Therefore, the couple (P_c, P_d) was associated to a couple (Q_c, Q_d) for each experiment.

Droplets volume V_{plot} and surface S_{plot} were deduced from droplets diameter using Nie et al. (2008) statement, assuming a spherical shape when unconstrained by channel walls, and a discoid shape when the diameter of an undeformed droplet is larger than the channel height (consistent with observations within the dripping regime in the used junctions):

$$V_{plot} = \begin{cases} \frac{4}{3}\pi\left(\frac{l_{plot}}{2}\right)^3 & \text{if } l_{plot} < h_{channel} \\ \frac{\pi}{12}(3 \times l_{plot}^2 h_{channel} - h_{channel}^3) & \text{if } h_{channel} < l_{plot} < w_{channel} \end{cases}, \tag{3}$$

and

$$S_{plot} = \begin{cases} 4\pi\left(\frac{l_{plot}}{2}\right)^2 & \text{if } l_{plot} < h_{channel} \\ \pi l_{plot} h_{channel} & \text{if } h_{channel} < l_{plot} < w_{channel} \end{cases}. \tag{4}$$

2.5 Identification of the flow regime of the study

To compare our results with the results of the literature, it was important to determine the flow regime to which belong the experimental points of our study.

In the case of T-junctions, in the dripping regime, one of the main empirical model was developed by Xu et al. (2006a, b, c, 2008) for a wide range of capillary numbers ($0.01 \leq Ca_c \leq 0.3$) (See supplementary material). Then, Ca_c -dependent flow maps determined by Xu et al. (2008) were used to locate our experimental points and our generation regimes. Given the limitations of the accessible flow-rates in the T-junctions detailed in Table 1 for the two chemical systems and according to Xu et al. (2008), most of our experiments belong to the dripping regime ($0.01 \leq Ca_c \leq 0.3$ —Fig. 4). As a consequence, models by Glawdel et al. (2012a, b)—though mostly effective in the transition regime—and Xu et al. were used to compare our datasets.

Regarding the X-junction (Fig. 5), our experiments are identified to belong mostly to the dripping regime, according to Nunes et al. (2013) cartography (see supplementary material) and within the limitations of the domain of use of the microsystems (Table 3). Then, the applicability of the model proposed in the current article will be limited to the dripping regime. Cubaud and Mason (2008), Liu and Zhang (2011) and Chen et al. (2014)—although this last one is mostly effective in the squeezing regime—models were therefore used to compare our datasets.

For the T and X-junctions and their domain of use of the given chemical systems (Table 2), we ensured the experiments were performed in the dripping regime and can be compared to other results obtained in the same flow regime in the literature. We note that for a particular chemical system and a given junction, not all the flow regimes are accessible.

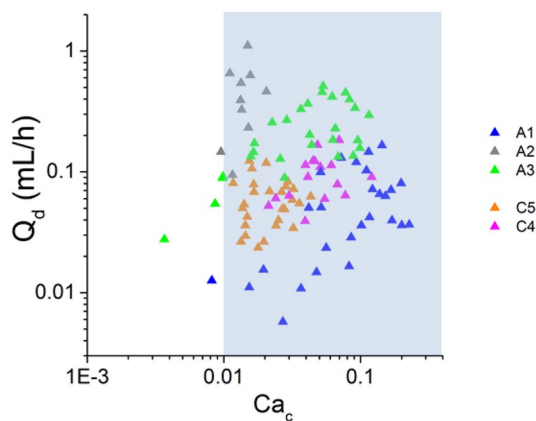


Fig. 4 Flow cartography for T-junctions—current data corresponding to A₁, A₂, A₃, C₄, C₅ global systems referring to both a junction type (Table 1) and a chemical system (Table 2)

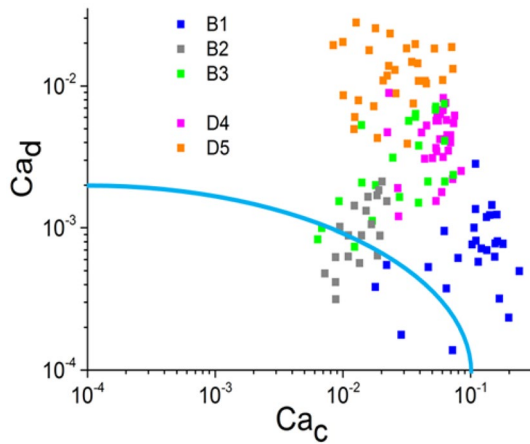


Fig. 5 Flow cartography for X-junctions—current data corresponding to B₁, B₂, B₃, D₄, D₅ global systems referring to both a junction type (Table 1) and a chemical system (Table 2)

3 Results and discussion

Once the experimental flow rates were demonstrated to belong to the dripping regime for the two junctions, the literature models proposed in these junctions were applied to these experimental points to evaluate their validity in our conditions. In the literature, two kinds of models are described: empirical and comprehensive models. These two kinds of model were studied separately. Unlike the other studies in the literature, results obtained in T and

$$\frac{l_{\text{plot}}}{h} = \begin{cases} 2.2 \times 10^{-4}(1 + \Phi) \times Ca_c^{-1} & \text{for } l_{\text{plot}} > 2.5h \\ 0.5(1 + \Phi)^{0.17} \times Ca_c^{-0.17} & \text{for } l_{\text{plot}} < 2.5h \end{cases} \text{ and } \Lambda = \Gamma = 1, \quad \lambda < \frac{1}{22}, \tag{8}$$

and

$$\frac{l_{\text{plot}}}{w_c} = (0.347 + 0.253\Phi) Ca_c^{-0.245} \text{ for } \Lambda = \Gamma = 1, \quad \lambda = (0.3; 0.6). \tag{9}$$

X-junctions with same aspect ratio were exploited grouped together.

Secondly, a new model was proposed and validated. This new model, assessing accurately the dependence towards both the flow-rate ratio and the capillary number of the continuous phase, was used to predict the characteristics of the segmented flow within the dripping regime, and the domain of use of the two junctions for the studied chemical systems.

3.1 Processing of the experimental results with the empirical models of the literature for the dripping regime

In the dripping regime, one of the main empirical model for the T-junction was developed by Xu et al. (2006a, b, c, 2008) (Eq. 7) for a wide range of capillary numbers ($0.01 \leq Ca_c \leq 0.2$). Xu et al. defined a modified capillary number to take into account the influence of the droplet size on the continuous phase velocity across the forming droplet:

$$Ca'_c = Ca_c \times \frac{w_c h}{w_c h - \frac{\pi}{4} \times l_{\text{plot}}^2}. \tag{5}$$

Hence,

$$\frac{l_{\text{plot}}}{w_c} \approx \frac{1}{Ca'_c} = \frac{1}{Ca_c} \times \left(\frac{w_c h - \frac{\pi}{4} \times l_{\text{plot}}^2}{w_c h} \right). \tag{6}$$

From Eq. (6), one can deduce

$$\frac{l_{\text{plot}}}{h} = Ca_c \times \left(\frac{-1 + \sqrt{1 + \frac{\pi w_c}{h Ca_c^2}}}{0.5\pi} \right). \tag{7}$$

For X-junctions, models by Cubaud and Mason (2008) (Eq. 8) and Liu and Zhang (2011) (Eq. 9) concluded that the normalized droplet diameter was a function of the flow-rate ratio and capillary number of the continuous phase, respectively,

It is worth pointing out that these models are defined for viscosity ratios well under 1 and close to 1, respectively.

Deviation between experimental data and empirical equations from Cubaud et al. and Liu et al. was investigated by plotting the experimental error as a function of the flow-rate ratio and capillary number of the continuous phase:

$$\text{Deviation (\%)} = 100 \times \frac{(l_{\text{plot}}/w_c)_{\text{exp}} - (l_{\text{plot}}/w_c)_{\text{th}}}{(l_{\text{plot}}/w_c)_{\text{th}}}. \tag{10}$$

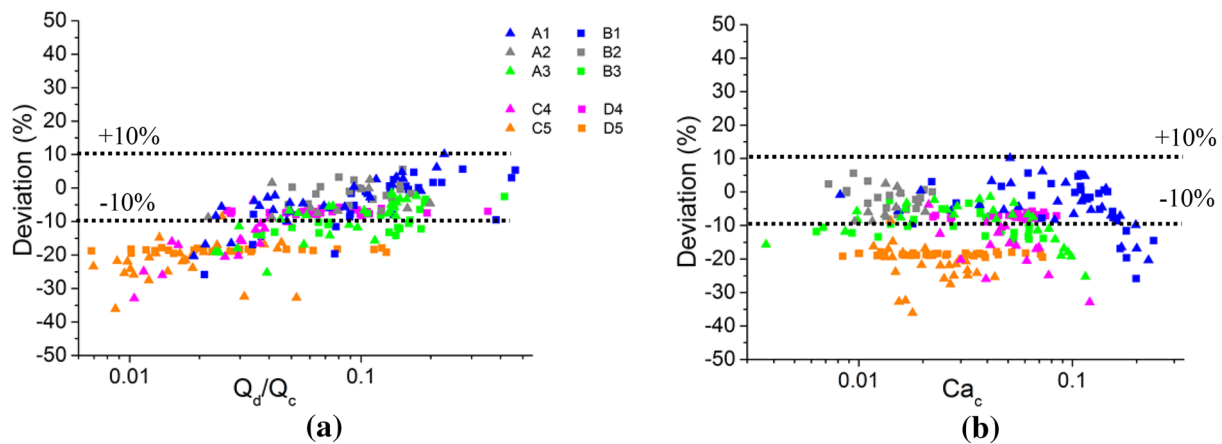


Fig. 6 Deviation of the experimental data towards Cubaud and Mason (2008) model (Eq. 8) as a function of the flow rate ratio (a) and capillary number of the continuous phase (b), for A₁, A₂, A₃, B₁, B₂, B₃, C₄, C₅, D₄, D₅ global systems

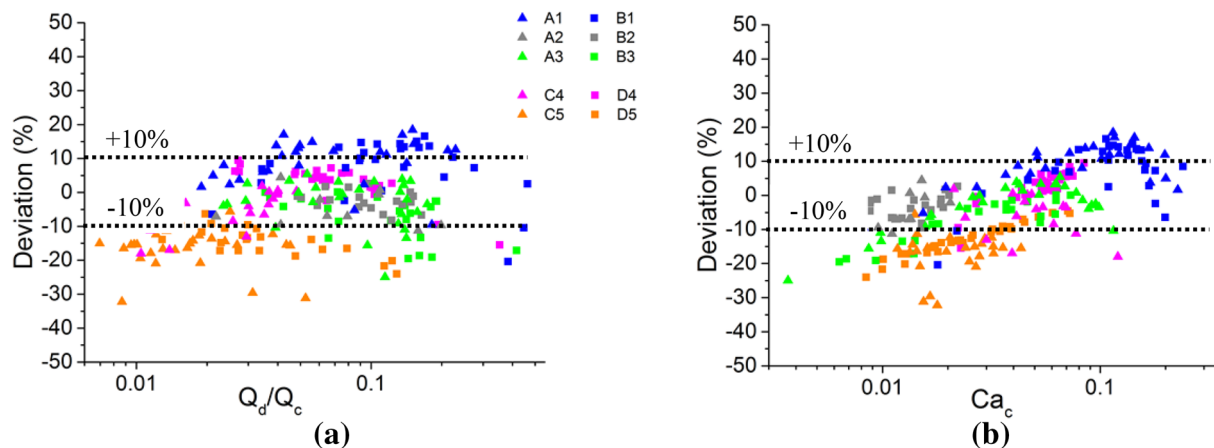


Fig. 7 Deviation of the experimental data towards Liu and Zhang (2011) model (Eq. 9) as a function of the flow rate ratio (a) and capillary number of the continuous phase (b), for A₁, A₂, A₃, B₁, B₂, B₃,

C₄, C₅, D₄, D₅ global systems referring to both a junction type (Table 1) and a chemical system (Table 2)

Droplets diameter, frequency, spacing and velocity were acquired for the ten global systems in the dripping regime (Sect. 2.4). Resulting deviations of the normalized droplet diameter are given in Figs. 6 and 7 as a function of the flow rate ratio Φ and the capillary number of the continuous phase. As predicted, Cubaud and Mason (2008) model (Eq. 8) was found to perform very well towards chemical systems with low viscosity ratios (i.e., 1, 2) while Liu et al. model (Eq. 9) performed accurately towards chemical systems with similar viscosities (i.e., 2, 3, 4) but both models failed to predict droplet generation when using viscous fluids as dispersed phase (5). Interestingly, the deviation was also found to be dependent towards the flow-rate ratio when data was compared with Cubaud et al. model while being dependent towards the capillary number when compared with Liu et al. model.

The empirical model by Xu et al. (2008) Eq. (7) was not plotted because drastically overestimating the diameter of the drops. This overestimation can be observed in Fig. 8.

A predictive model for high viscosity ratios, assessing accurately the dependence towards both the flow-rate ratio and the capillary number of the continuous phase has, therefore still to be developed.

3.2 Description of the comprehensive models developed for near-dripping regime in T and X-junctions

There is only one comprehensive model developed in T-junctions to describe the transition regime close to the dripping regime. Despite this, we used it to process our results. In T-junction, comprehensive models were first developed by van

Steijn et al. (2010) in the squeezing regime and Glawdel et al. (2012a, b) (Eq. 11) in the transition regime. This last model is not only validated for their datasets, but applicable to any set of experiments performed in T-junctions for $Ca_c < 0.005$ and $\lambda \leq 1.7$. As such, we expect an overestimation of the result obtained in the dripping regime, as the influence of the capillary number will be more prominent. Similarly to van Steijn et al., Glawdel et al. (2012a, b) defined the normalized volume of the droplet as a sum of the contribution of lag, filling and necking stages:

$$\frac{V_{plot}}{hw_c^2} = \alpha_{lag} + \alpha_{fill} + \beta\Phi, \tag{11}$$

where α_{lag} and α_{fill} are the volumes added respectively during the lag and filling stages, and β the dimensionless necking time. Then, using geometrical considerations, based on the observation of droplet generation, Glawdel et al. (2012a, b) defined a system of equations for α_{lag} , α_{fill} , and β that can be solved to deduce the volume of the droplets.

In X-junctions, Chen et al. (2014) created a similar comprehensive model based on the resolution of a system of equations derived from geometrical considerations, just removing the occurrence of the lag stage:

$$\frac{V_{plot}}{hw_c^2} = \alpha_{fill} + \beta\Phi. \tag{12}$$

Although defined for the squeezing regime, Chen model (i.e., Eq. 12) was found to be quite effective to model our

experiments in the dripping regime, although a small overestimation occurred, as expected (Fig. 8).

3.3 New model proposal for the T and X-junctions within the dripping regime

To complement existing models in the dripping regime, the following model was developed for $\Lambda = \Gamma = 1$, $0.056 < \lambda < 17.92$ suitable for both T and X-junction:

$$\frac{l_{plot}}{w_c} = \chi_1 \Phi^{\chi_2} Ca_c^{\chi_3}. \tag{13}$$

A fit was carried out on global systems excluding C_4 and D_4 , used to validate our model. The values of the fitting parameters are given in Table 4. Interestingly, the value of fitting parameter χ_3 was found to be very close to the one described by Cubaud and Mason (2008) (Eq. 8). However, the influence of the flow-rate ratio on the normalized diameter of the droplets was found to be even smaller than what was shown in previous studies, probably because of the expansion of the outlet microchannel after the used junction. The flow-rate ratio has a minor

Table 4 Value of fitting parameters for Eq. (13), $\Lambda = \Gamma = 1$, $0.056 < \lambda < 17.92$, for $A_1, A_2, A_3, B_1, B_2, B_3, C_5, D_5$ experiments obtained in both T and X-junctions, $R^2 = 0.88$

Parameters	χ_1	χ_2	χ_3
Value	0.605	0.085	-0.158
Standard error	0.015	0.005	0.005

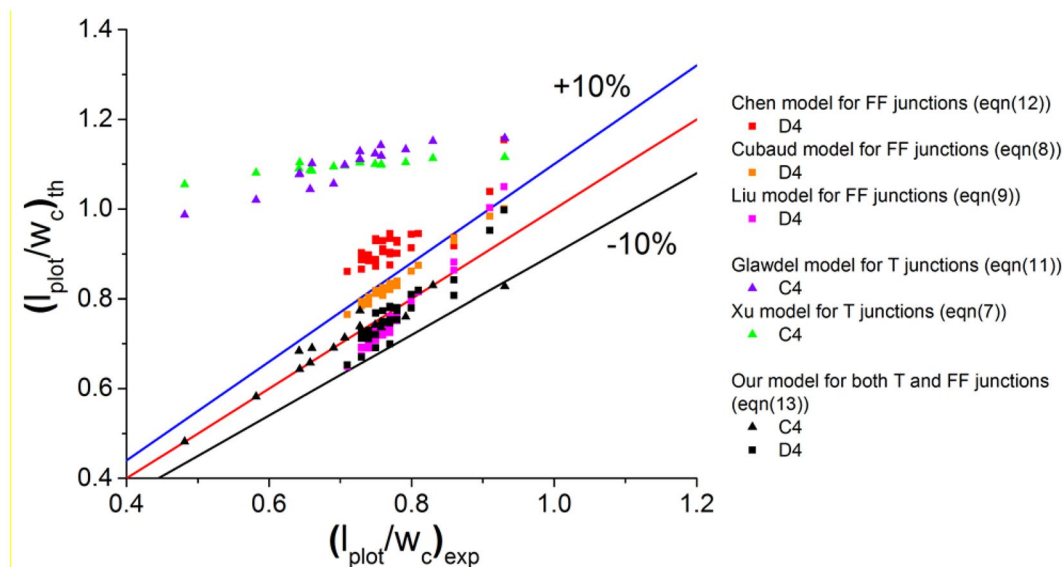


Fig. 8 Parity plot of the non-dimensional droplet diameter between the predicted results and experimental data issued from C_4 and D_4 global systems. C_4 and D_4 global systems refer to both a junction type (Table 1) and a chemical system (Table 2)

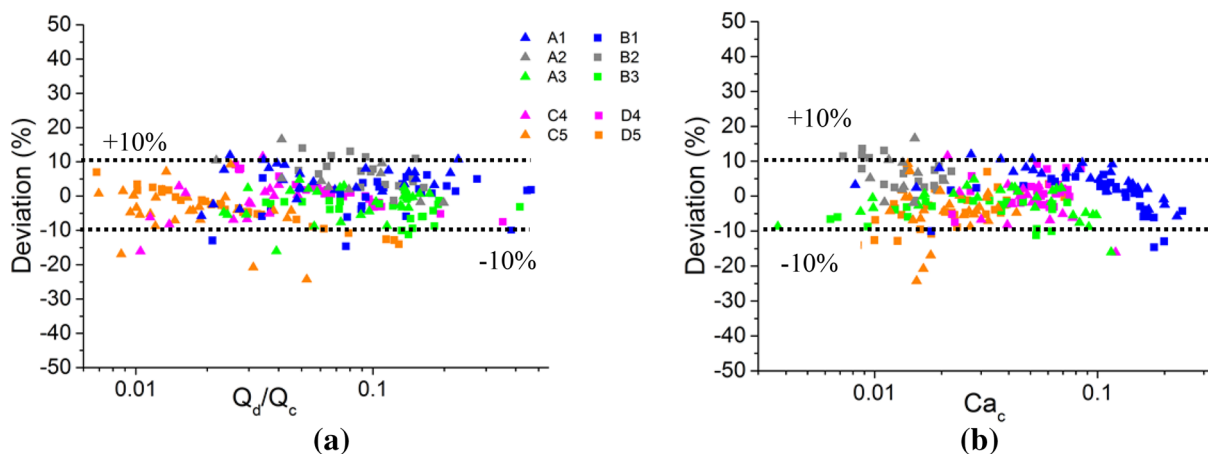


Fig. 9 Deviation of the experimental data towards our model (Eq. 13) as a function of the flow rate ratio (a) and capillary number of the continuous phase (b), for A₁, A₂, A₃, B₁, B₂, B₃, C₄, C₅, D₄, D₅ global

systems referring to both a junction type (Table 1) and a chemical system (Table 2)

impact on the droplet diameter. When trying to create a specifically designed dispersion in the dripping regime, one should therefore, first focus on the capillary number (i.e., flow-rate for a given global system) of the continuous phase to choose a specific droplet diameter, then adjust the flow-rate ratio to optimize the droplet spacing/frequency. Finally, the viscosity ratio was surprisingly found not to influence droplet generation, contrary to previous results from the literature (Gupta et al. 2009). A possible reason could be that the flow-rate ratios we tested were mostly below 0.3. As a consequence, the viscous force of the dispersed phase remained small, even for relatively high viscosity ratios. However, within the scope of this study,

large flow-rate ratios were not tested because they led to droplet coalescence (Fig. 10a).

3.4 Model validation

Figure 8, we can observe the good agreement of the model (Eq. 13) with the experimental results obtained for the global systems C₄ and D₄ ($\lambda = 1.099$). Interestingly, no difference was found between T-junctions and X-junctions. Therefore, the model is able to predict accurately the droplet diameter for both types of junctions. We can assume that when considering the dripping regime, in which the effect of the capillary number is predominant over the flow-rate ratio, only the sum of the forces exerted on the to-be-dispersed fluid is to

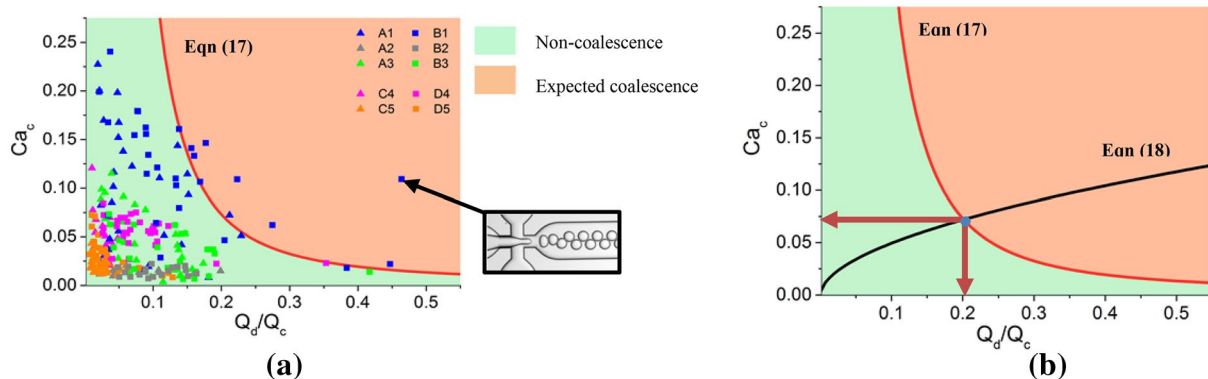


Fig. 10 a Mathematical prediction of the accessible flow rate ratio and capillary number ranges, for A₁, A₂, A₃, B₁, B₂, B₃, C₄, C₅, D₄, D₅ global systems; the green surface corresponding to the accessible phase. Arrows indicating the maximum capillary number and flow-rate ratio achievable when respecting Eqs. (17) and (18), with $(l_{plot}/w_c)_{targeted} = 0.8$. (Color figure online)

diameter. Red curve following Eq. (17). Green surface showing accessible flow-rate ratio and capillary number of the continuous phase. Arrows indicating the maximum capillary number and flow-rate ratio achievable when respecting Eqs. (17) and (18), with $(l_{plot}/w_c)_{targeted} = 0.8$. (Color figure online)

be considered, and not the way it is exerted (by a T or a FF junction). Such a hypothesis would have a significant impact on the understanding of droplet generation, hence further research is needed to confirm it.

Liu et al. (Eq. 9) and Cubaud and Mason (2008) (Eq. 8) models also predict pretty accurately our results (within 10% deviation). The empirical model of Xu et al. in the dripping regime (Eq. 7) overestimates all our results, and quite correlates with Glawdel global model (Eq. 11) defined as truly effective in the transition regime. As expected, Chen et al. (2014) global model (Eq. 12) of droplet generation in FF-junctions in the squeezing regime overestimates the results. However, the prediction is not totally irrelevant, as most predictions remain within 20% deviation of experimental data.

Once validated using C₄ and D₄ control systems, the model deviation towards the experimental results is recapitulated (Fig. 9). The comparison of the results presented Fig. 9 with Figs. 6 and 7 highlights the benefits of the new model within the dripping regime. It is suitable for the two junctions as long as the aspect ratio is equal to 1 and to biphasic chemical systems with a larger range of viscosity ratios (0.056 < λ < 17.92).

For various pairs of flow-rates, we represented droplet generation on Table 5, and calculated the relative error induced by Eq. (13). Droplet generation in X-junctions, compared to T-junctions, allows the use of higher flow-rate ratios Φ. Though droplets generation may be independent of the used junction for a given flow-rate ratio and capillary number of the continuous phase, the accessible range of these two variables will vary depending on the used junction. During our study, we found the X-junction to be more polyvalent, and accessible ranges to be wider than in T-junctions.

3.5 Predictive scope of the model

In this section, the new model is used to predict the characteristics of the segmented flow within the dripping regime and the domain of use of the two junctions for the studied chemical systems. Then, the optimized specific interfacial area accessible for our chemical systems in these junctions is determined.

3.5.1 Deriving droplet population characteristics using the new comprehensive model

Beyond a simple computation of a droplet length, Eq. (13) enables the user to determine the whole characteristics of the droplet population.

Combining Eqs. (3) and (13), one can deduce the dependence of the droplet volume towards the flow rate ratio and the capillary number of the continuous phase. The same can be done combining Eqs. (4) and (13) for the surface of the droplets. For simplification means, we assume the following expression of the velocity of unconfined droplets (Sessoms et al. 2009):

$$v_{\text{plot}} = \bar{\beta} \times \frac{(Q_c + Q_d)}{h_{\text{channel}} w_{\text{channel}}} \tag{14}$$

With $\bar{\beta}$ a parameter depending on the microchannel geometry and the viscosity ratio whose value is comprised between 1 and 2. We evaluated this parameter to be about 1.8 for the HNO₃/DMDBTDMA chemical system and 1.5 for the HCl/Aliquat® 336 one. To simplify the discussion, we decided to take 1.5 for both chemical systems.

As a consequence, the spacing between consecutive droplets can be calculated by:

Table 5 Examples of droplet generation for the C₄ and D₄ global systems referring to both a junction type (Table 1) and a chemical system (Table 2), relative error of Eq. (13)

Global system	(Q _c , Q _d) (mL h ⁻¹) ²	Picture	Mean droplet diameter (μm)	Predicted droplet diameter (μm)	$\frac{\Delta r}{r}$ (%)
C4	(3.23, 0.12)		74.9 ± 2.1	74.2	0.9
C4	(1.73, 0.06)		83.0 ± 2.1	81.3	2.0
D4	(3.25, 0.35)		80.0 ± 2.1	80.9	1.1
D4	(1.65, 0.58)		93.0 ± 2.1	99.7	7.2

$$s = \frac{v_{\text{plot}}}{f} = \frac{1.5(Q_c + Q_d)}{h_{\text{channel}} w_{\text{channel}} f}. \quad (15)$$

Combining Eqs. (2) and (15), the spacing was shown as a function of the flow-rate ratio and the volume of the droplet:

$$s = 1.5 \frac{V_{\text{plot}}}{h_{\text{channel}} w_{\text{channel}}} \left(1 + \frac{1}{\Phi}\right). \quad (16)$$

This expression allowed us to predict accurately coalescence, whenever $s = l_{\text{plot}}$, by combining Eqs. (16) and (13). Assuming droplets have a spherical shape:

$$s = l_{\text{plot}} \text{ if and only if } \text{Ca}_c = \left(\frac{1}{\chi_1 \times \phi^{\chi_2}} \sqrt{\frac{4 w_{\text{channel}} \phi}{\pi w_c (1 + \phi)}} \right)^{1/\chi_3}. \quad (17)$$

The quick calculation made to derive the spacing from the volume of the droplet enabled us to predict coalescence, and therefore, to find the accessible pairs of (Φ, Ca_c) within the dripping regime, for our junctions. On Fig. 10a, the tested (Φ, Ca_c) pairs are plotted, for the ten global systems. The empirical Eq. (13) is used to differentiate the accessible pairs, i.e., the domain of use of the two junctions for the studied chemical systems, with a separation whenever $s = l_{\text{plot}}$, to take into account coalescence. We can observe that most of the experimental data are located on the green surface corresponding to the predicted accessible dripping regime. Therefore, the determination of the spacing was achievable for our given chemical systems, and flow-rate ratio and capillary number ranges that were found experimentally could be retrieved theoretically (Table 3). Using this model, future users may identify a priori flow-rate ranges for given physicochemical properties of their phases and geometry of their chip. With only a few exceptions for B_1 (Fig. 10a) as high flow-rate ratios and capillary numbers were experienced, the maximum tested flow-rate ratio and capillary numbers recorded in Table 3 belong to the green surface. Indeed, when creating droplet populations, we made care to avoid coalescence by imposing $s > l_{\text{plot}}$ as no surfactant was added.

Repercussions of this calculation are multiple. When creating droplets, one may want to target a specific droplet diameter while changing their generation frequency. Using the new model, the flow-rate ratio and capillary number of the dispersed phase can easily be modified to meet these needs. To do so, following Eq. (13), the capillary number and flow-rate ratio must be changed accordingly:

$$\text{Ca}_c = \left(\frac{\left(l_{\text{plot}}/w_c \right)_{\text{targeted}}}{\chi_1} \times \Phi^{-\chi_2} \right)^{1/\chi_3}. \quad (18)$$

Combining Eq. (18) and previous determination of the accessible flow-rate ratio and capillary number ranges to avoid coalescence, Fig. 10 b. can be plotted for $\left(l_{\text{plot}}/w_c \right)_{\text{targeted}} = 0.8$.

Droplet diameter conservation is possible if every increase in the flow-rate ratio is compensated by an increase in the capillary number of the continuous phase, while avoiding coalescence. For a given chemical system, this results in a joint increase in both flow rates, though higher for the dispersed phase than the continuous one.

3.5.2 Specific interfacial area calculation

Finally, the specific interfacial area was defined as the ratio between the area of a droplet and the volume in which it is comprised within the microchannel:

$$S_{\text{int,specific}} = \frac{S_{\text{plot}}}{h_{\text{channel}} w_{\text{channel}} s}. \quad (19)$$

The resulting plot for the accessible pairs of (Φ, Ca_c) is given in Fig. 11. By adjusting this plot, one may determine how to optimize the specific interfacial area, for a given microchannel geometry. In our microsystems, over the studied pairs of (Φ, Ca_c) , relatively low capillary numbers of the continuous phase and high flow-rate ratios shall be used, so that the spacing between consecutive droplets has to be as short as possible. Note however that, within our microsystems, due to low $\left(\Gamma = \frac{1}{3} \right)$ aspect ratio in the outlet microchannel, considering Eq. (19), the maximum specific interfacial area reached only about $10,000 \text{ m}^{-1}$, which was already reached in parallel flows by Hellé et al. (2014) for the same chemical systems, though mass transfer is expected to be enhanced in segmented flows for the same interfacial area due to recirculation patterns within droplets and slugs (Burns and Ramshaw 2001).

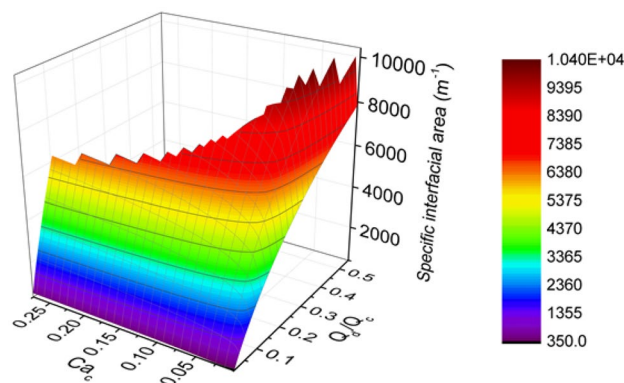


Fig. 11 Specific interfacial area calculation within the studied microsystem, with no specification on the used junction (T, X) for the defined range of viscosity ratio $0.056 < \lambda < 17.92$

4 Conclusion

In this study, droplet generation was thoroughly investigated, through the use of two chemical systems and for different microchannels differing from their hydrophobicity and junction type. For every chemical system, both O/W and W/O flows were carried out. Droplet population characteristics were acquired and compared. Interestingly, when plotted as a function of the flow-rate ratio and the capillary number of the continuous phase, droplet diameters were found to collapse on a single master curve, with no influence arising from the used junction type, hydrophobicity of the microchannel, or chemical system. As current empirical equations in the literature were found to be not sufficiently accurate towards high viscosity ratio chemical systems, a simple comprehensive model was developed for the normalized diameter/length of the droplets, as a function of the flow-rate ratio and the capillary number of the continuous phase and validated. The newly developed empirical equation (Eq. 13) was validated for both type of junctions (T, X) as long as the aspect ratio is equal to 1 and to biphasic chemical system for a larger range of viscosity ratios ($0.056 < \lambda < 17.92$). It enabled the prediction of the domain of use of the microchip at first and second, droplets diameter, volume, spacing, and specific interfacial area. Specific interfacial area could be optimized using the model within our specific microsystems, and a maximum of $10,000 \text{ m}^{-1}$ was determined. Knowing how to predict and optimize the specific interfacial area is a key to the improvement of liquid–liquid extraction, currently performed in multiple industries as varied as hydrometallurgy and the nuclear, petrochemical, pharmaceutical and agri-food industries. Ensuing the definition of the model, several insights in the way to optimize segmented flows for different purposes were proposed, i.e., for the production of monodisperse populations of droplets and mass transfer optimization.

Several assumptions were made however, that can diminish the predictability of the model. The first one is the definition of the mean velocity of the droplets. Indeed, we assumed a very simple definition for the droplet velocity, not to add an additional complication. However, one might be interested to add a more thorough definition for the droplet velocity using empirical correlations for the terminal velocity depending on the drag coefficient (Wegener et al. 2014). Also, experiments were performed at relatively low interfacial tension between the continuous and to-be-dispersed phases, and surfactants may influence droplet formation through Marangoni stresses (Baret et al. 2009; van Loo et al. 2016). When operating with surfactants, one might expect a deviation from our empirical equation.

As a perspective, please note that the model developed in this article would need further testing, by varying the dimensions of the junction—while keeping $\Gamma = \Lambda = 1$

—and further adaptation when varying the aspect ratio and the dispersed-to-continuous channel width ratio. Also note that comprehensive models for the dripping regime, as those developed by Glawdel et al. (2012a, b) (Eq. 11) in the transition regime for the T-junction and by Chen et al. (2014) (Eq. 12) in the squeezing regime for the X-junction, are still needed for both T and X-junctions.

Acknowledgements This work was supported by the French Alternative Energies and Atomic Energy Commission. We would like to thank Amar Basu (Electrical and Computer Engineering, Wayne State University, Michigan) for providing us the DMV software we used to acquire droplets shapes and velocities.

References

- Ahmed B, Barrow D, Wirth T (2006) Enhancement of reaction rates by segmented fluid flow in capillary scale reactors. *Adv Synth Catal* 348(9):1043–1048
- Anna SL (2016) Droplets and bubbles in microfluidic devices. *Annu Rev Fluid Mech* 48(1):285–309
- Aota A, Nonaka M, Hibara A, Kitamori T (2007) Countercurrent laminar microflow for highly efficient solvent extraction. *Angew Chem Int Ed Engl* 46(6):878–880
- Assmann N, Ładosz A, Rudolf von Rohr P (2013) Continuous micro liquid–liquid extraction. *Chem Eng Technol* 36(6):921–936
- Baret JC, Kleinschmidt F, El Harrak A, Griffiths AD (2009) Kinetic aspects of emulsion stabilization by surfactants: a microfluidic analysis. *Langmuir* 25(11):6088–6093
- Basu AS (2013) Droplet morphometry and velocimetry (DMV): a video processing software for time-resolved, label-free tracking of droplet parameters. *Lab Chip* 13(10):1892–1901
- Boyd-Moss M, Baratchi S, Di Venere M, Khoshmanesh K (2016) Self-contained microfluidic systems: a review. *Lab Chip* 16(17):3177–3192
- Burns JR, Ramshaw C (2001) The intensification of rapid reactions in multiphase systems using slug flow in capillaries. *Lab Chip* 1(1):10–15
- Chen X, Glawdel T, Cui N, Ren CL (2014) Model of droplet generation in flow focusing generators operating in the squeezing regime. *Microfluid Nanofluid* 18(5–6):1341–1353
- Chong ZZ, Tan SH, Ganan-Calvo AM, Tor SB et al (2015) Active droplet generation in microfluidics. *Lab Chip* 16(1):35–58
- Chong ZZ, Tor SB, Gañán-Calvo AM, Chong ZJ et al. (2016) Automated droplet measurement (ADM): an enhanced video processing software for rapid droplet measurements. *Microfluid Nanofluid* 20(4):66
- Christopher GF, Anna SL (2007) Microfluidic methods for generating continuous droplet streams. *J Phys D Appl Phys* 40(19):R319–R336
- Cubaud T, Mason TG (2008) Capillary threads and viscous droplets in square microchannels. *Phys Fluids* 20(5):053302
- Dreyfus R, Tabeling P, Willaime H (2003) Ordered and disordered patterns in two-phase flows in microchannels. *Phys Rev Lett* 90(14):144505
- Fries DM, Voith T, von Rohr PR (2008) Liquid extraction of vanillin in rectangular microreactors. *Chem Eng Technol* 31(8):1182–1187
- Fu T, Wu Y, Ma Y, Li HZ (2012) Droplet formation and breakup dynamics in microfluidic flow-focusing devices: from dripping to jetting. *Chem Eng Sci* 84:207–217

- Garstecki P, Stone HA, Whitesides GM (2005) Mechanism for flow-rate controlled breakup in confined geometries: a route to monodisperse emulsions. *Phys Rev Lett* 94(16):164501
- Garstecki P, Fuerstman MJ, Stone HA, Whitesides GM (2006) Formation of droplets and bubbles in a microfluidic T-junction—scaling and mechanism of break-up. *Lab Chip* 6(3):437–446
- Glawdel T, Elbuken C, Ren CL (2012a) Droplet formation in microfluidic T-junction generators operating in the transitional regime. I. Experimental observations. *Phys Rev E Stat Nonlinear Soft Matter Phys* 85(1 Pt 2):016322
- Glawdel T, Elbuken C, Ren CL (2012b) Droplet formation in microfluidic T-junction generators operating in the transitional regime. II. Modeling. *Phys Rev E Stat Nonlinear Soft Matter Phys* 85(1 Pt 2):016323
- Gupta A, Kumar R (2009) Effect of geometry on droplet formation in the squeezing regime in a microfluidic T-junction. *Microfluid Nanofluid* 8(6):799–812
- Gupta A, Kumar R (2010) Flow regime transition at high capillary numbers in a microfluidic T-junction: viscosity contrast and geometry effect. *Phys Fluids* 22(12):122001
- Gupta A, Murshed SMS, Kumar R (2009) Droplet formation and stability of flows in a microfluidic T-junction. *Appl Phys Lett* 94(16):164107
- Gupta A, Matharoo HS, Makkar D, Kumar R (2014) Droplet formation via squeezing mechanism in a microfluidic flow-focusing device. *Comput Fluids* 100:218–226
- Hatakeyama T, Chen DL, Ismagilov RF (2006) Microgram-scale testing of reaction conditions in solution using nanoliter plugs in microfluidics with detection by MALDI-MS. *J Am Chem Soc* 128(8):2518–2519
- Hellé G, Mariet C, Cote G (2014) Liquid–liquid microflow patterns and mass transfer of radionuclides in the systems Eu(III)/HNO₃/DMDBTDMMA and U(VI)/HCl/Alquat® 336. *Microfluid Nanofluid* 17(6):1113–1128
- Hessel V, Angeli P, Graviillidis A, Löwe H (2005) Gas–liquid and gas–liquid–solid microstructured reactors: contacting principles and applications. *Ind Eng Chem Res* 44:9750–9769
- Kashid MN, Renken A, Kiwi-Minsker L (2011) Influence of flow regime on mass transfer in different types of microchannels. *Ind Eng Chem Res* 50(11):6906–6914
- Kole S, Bikkina P (2017) A parametric study on the application of microfluidics for emulsion characterization. *J Petrol Sci Eng* 158:152–159
- Kralj JG, Sahoo HR, Jensen KF (2007) Integrated continuous microfluidic liquid–liquid extraction. *Lab Chip* 7(2):256–263
- Liu H, Zhang Y (2009) Droplet formation in a T-shaped microfluidic junction. *J Appl Phys* 106(3):034906
- Liu H, Zhang Y (2011) Droplet formation in microfluidic cross-junctions. *Phys Fluids* 23(8):082101
- Nie Z, Seo M, Xu S, Lewis PC et al (2008) Emulsification in a microfluidic flow-focusing device: effect of the viscosities of the liquids. *Microfluid Nanofluid* 5(5):585–594
- Nunes JK, Tsai SS, Wan J, Stone HA (2013) Dripping and jetting in microfluidic multiphase flows applied to particle and fiber synthesis. *J Phys D Appl Phys* 46(11):114002
- Romero PA, Abate AR (2012) Flow focusing geometry generates droplets through a plug and squeeze mechanism. *Lab Chip* 12(24):5130–5132
- Sen N, Darekar M, Singh KK, Mukhopadhyay S et al (2014) Solvent extraction and stripping studies in microchannels with TBP nitric acid system. *Solvent Extr Ion Exch* 32(3):281–300
- Sessoms DA, Belloul M, Engl W, Roche M et al (2009) Droplet motion in microfluidic networks: Hydrodynamic interactions and pressure-drop measurements. *Phys Rev E Stat Nonlinear Soft Matter Phys* 80(1 Pt 2):016317
- Shui L, Eijkel JC, van den Berg A (2007) Multiphase flow in microfluidic systems—control and applications of droplets and interfaces. *Adv Colloid Interface Sci* 133(1):35–49
- Song H, Tice JD, Ismagilov RF (2003) A microfluidic system for controlling reaction networks in time. *Angew Chem Int Ed Engl* 42(7):767–772
- Song H, Chen DL, Ismagilov RF (2006) Reactions in droplets in microfluidic channels. *Angew Chem Int Ed Engl* 45(44):7336–7356
- Tice JD, Lyon AD, Ismagilov RF (2004) Effects of viscosity on droplet formation and mixing in microfluidic channels. *Anal Chim Acta* 507(1):73–77
- Umbanhowar PB, Prasad V, Weitz DA (2000) Monodisperse emulsion generation via drop break off in a coflowing stream. *Langmuir* 16:347–351
- Utada AS, Fernandez-Nieves A, Stone HA, Weitz DA (2007) Dripping to jetting transitions in coflowing liquid streams. *Phys Rev Lett* 99(9):094502
- van Steijn V, Kleijn CR, Kreutzer MT (2010) Predictive model for the size of bubbles and droplets created in microfluidic T-junctions. *Lab Chip* 10(19):2513–2518
- van Loo S, Stoukatch S, Kraft M, Gilet T (2016) Droplet formation by squeezing in a microfluidic cross-junction. *Microfluid Nanofluid* 20(10):146
- Wegener M, Paul N, Kraume M (2014) Fluid dynamics and mass transfer at single droplets in liquid/liquid systems. *Int J Heat Mass Transf* 71:475–495
- Xu JH, Li SW, Tan J, Wang YJ et al (2006a) Controllable preparation of monodisperse O/W and W/O emulsions in the same microfluidic device. *Am Chem Soc* 22:7243–7246
- Xu JH, Li SW, Tan J, Wang YJ et al (2006b) Preparation of highly monodisperse droplet in a T-junction microfluidic device. *AIChE J* 52(9):3005–3010
- Xu JH, Luo GS, Li SW, Chen GG (2006c) Shear force induced monodisperse droplet formation in a microfluidic device by controlling wetting properties. *Lab Chip* 6(1):131–136
- Xu JH, Li SW, Tan J, Luo GS (2008) Correlations of droplet formation in T-junction microfluidic devices: from squeezing to dripping. *Microfluid Nanofluid* 5(6):711–717
- Zheng B, Ismagilov RF (2005) A microfluidic approach for screening submicroliter volumes against multiple reagents by using preformed arrays of nanoliter plugs in a three-phase liquid/liquid/gas flow. *Angew Chem Int Ed* 44(17):2520–2523
- Zhu P, Wang L (2016) Passive and active droplet generation with microfluidics: a review. *Lab Chip* 17(1):34–75

Publisher's Note Springer Nature remains neutral with regard to jurisdictional claims in published maps and institutional affiliations.